



FULL LENGTH ARTICLE

LncRNA H19 mediates BMP9-induced angiogenesis in mesenchymal stem cells by promoting the p53-Notch1 angiogenic signaling axis

Chengcheng Du ^{a,b}, Qiang Cheng ^{a,b}, Piao Zhao ^{b,c},
 Claire Wang ^d, Zhenglin Zhu ^{a,b}, Xiangdong Wu ^e,
 Shengqiang Gao ^{a,b}, Bowen Chen ^{a,b}, Jing Zou ^{a,b},
 Wei Huang ^{a,b,**}, Junyi Liao ^{a,b,*}

^a Department of Orthopedic Surgery, The First Affiliated Hospital of Chongqing Medical University, Chongqing 400016, China

^b Orthopedic Laboratory of Chongqing Medical University, Chongqing 400016, China

^c Molecular Oncology Laboratory, Department of Orthopedic Surgery and Rehabilitation Medicine, The University of Chicago Medical Center, Chicago, IL 60637, USA

^d Department of Computational and Applied Mathematics, Rice University, Houston, TX 77005, USA

^e Department of Orthopedic Surgery, Peking Union Medical College Hospital, Chinese Academy of Medical Sciences & Peking Union Medical College, Beijing 100730, China

Received 19 February 2022; received in revised form 30 March 2022; accepted 27 April 2022

Available online 10 May 2022

KEYWORDS

Angiogenesis;
 BMP9;
 Bone tissue
 engineering;
 LncRNA H19;
 Mesenchymal stem
 cells

Abstract BMP9 mediated osteogenic differentiation mechanisms of MSCs were widely explored, however, mechanisms of BMP9-induced angiogenesis still need to be clarified. We previously characterized that Notch1 promoted BMP9-induced osteogenesis–angiogenesis coupling process in mesenchymal stem cells (MSCs). Here, we explored the underlying mechanisms of lncRNA H19 (H19) mediated regulation of BMP9-induced angiogenesis through activating Notch1 signaling. We demonstrated that basal expression level of H19 was high in MSCs, and silencing H19 attenuates BMP9-induced osteogenesis and angiogenesis of MSCs both *in vitro* and *in vivo*. Meanwhile, we identified that BMP9-induced production of CD31⁺ cells was indispensable for BMP9-induced bone formation, and silencing H19 dramatically blocked BMP9-

* Corresponding author. Department of Orthopedic Surgery, The First Affiliated Hospital of Chongqing Medical University, Chongqing 400016, China. Fax: +86 23 89011211.

** Corresponding author. Department of Orthopedic Surgery, The First Affiliated Hospital of Chongqing Medical University, Chongqing 400016, China. Fax: +86 23 89011211.

E-mail addresses: huangwei68@263.net (W. Huang), liaojunyi@cqmu.edu.cn (J. Liao).

Peer review under responsibility of Chongqing Medical University.

<https://doi.org/10.1016/j.gendis.2022.04.013>

2352-3042/© 2022 The Authors. Publishing services by Elsevier B.V. on behalf of KeAi Communications Co., Ltd. This is an open access article under the CC BY-NC-ND license (<http://creativecommons.org/licenses/by-nc-nd/4.0/>).

induced production of CD31⁺ cells. In addition, we found that down-regulation of H19 inhibited BMP9 mediated blood vessel formation and followed subsequent bone formation *in vivo*. Mechanistically, we clarified that H19 promoted p53 phosphorylation by direct interacting and phosphorylating binding, and phosphorylated p53 potentiated Notch1 expression and activation of Notch1 targeting genes by binding on the promoter area of *Notch1* gene. These findings suggested that H19 regulated BMP9-induced angiogenesis of MSCs by promoting the p53-Notch1 angiogenic signaling axis.

© 2022 The Authors. Publishing services by Elsevier B.V. on behalf of KeAi Communications Co., Ltd. This is an open access article under the CC BY-NC-ND license (<http://creativecommons.org/licenses/by-nc-nd/4.0/>).

Introduction

Bone defects and nonunion of fractures are complicated clinical problems which cause great burdens for both patients and health care system. Treatment of these problems requires desirable osteoinductive, osteoconductive, osteogenic and angiogenic properties for formation of robust and mature bone.^{1–3} Bone morphogenetic protein 9 (BMP9), also known as growth differentiation factor 2 (GDF2), is characterized as one of most potential BMPs for mesenchymal stem cells (MSCs) mediated bone regeneration.^{4–9} Besides osteoinductive, osteoconductive and osteogenic properties, BMP9 mediated angiogenic potential is one of the most essential features distinguish from other BMPs.^{5,10} BMP9 mediated osteogenic differentiation mechanisms of MSCs were widely explored, however, mechanisms of BMP9 induced angiogenesis are still not clear. To clarify the mechanisms of BMP9-induced angiogenesis of MSCs, we found that Notch1 promoted BMP9-induced osteogenesis–angiogenesis coupling by both *in vitro* and *in vivo* experiments.⁵ However, BMP9 mediated Notch1 signaling activation in MSCs is far from clarified.

Recently, with the completion of the Human Genome Project, the emerging regulatory roles of non-coding RNAs (ncRNAs), especially lncRNAs are proved to be involved in many physiological and/or pathological processes.^{11–13} Long non-coding RNA H19 (LncRNA H19, H19) was identified as one of the first imprinted genes and lncRNAs as early as 1980s,^{14–16} which was characterized regulating tumorigenesis, embryo growth, stem cell differentiation etc.^{17–19} Correspondingly, several studies have identified the regulatory function of H19 in osteogenic differentiation of MSCs and the mechanisms still need to be further addressed.^{20–23} We previously reported that H19 participated in BMP9-induced osteogenic differentiation through activating Notch1 signaling and functioned as competing endogenous RNAs (ceRNAs).⁶ Furthermore, we identified that H19 regulates BMP2-induced hypertrophic differentiation of MSCs by promoting Runx2 phosphorylation.²⁴ Therefore, we speculated the regulatory properties of H19 in BMP9-induced angiogenesis of MSCs.

P53 also known as *TP53*, which is a classic tumor suppressor gene functioned in apoptosis, cell cycle arrest, and senescence etc. in response to distinct stimuli. Although the regulatory function of p53 in cell growth after exposure to stress has been well established, the function of p53 in metabolism and other biological processes including MSCs

differentiation is not totally clarified.^{25–28} Of note, as regulators of both tumorigenesis and MSCs differentiation, the crosstalk between p53 and H19 is worth to be clarified.^{29,30} Recently, it was reported that p53 mutant impaired H19 mediated osteogenic differentiation of osteoblast³⁰ and H19 hold the potential of regulating the stabilization of p53.³¹ Furthermore, several researches identified the directly or indirectly interaction between H19 and p53.^{32–34} These results indicated the regulatory function of H19 in the activation of p53 signaling.

In the present study, we identified the regulatory function of H19 in BMP9-induced angiogenesis of MSCs. We found that BMP9-induced angiogenesis of MSCs was characterized by increasing the production of CD31⁺ cells, silencing H19 blocked BMP9-induced angiogenesis and further attenuated BMP9-induced bone formation. Mechanistically, we clarified that H19 regulated BMP9-induced angiogenesis by directly interacting with p53 and promoting p53 phosphorylation, phosphorylated p53 further activated Notch1 transcription and triggered angiogenesis of MSCs. These findings provide insight into the mechanisms of H19 regulated BMP9-induced angiogenesis of MSCs, which is beneficial for the construction of BMP9-mediated bone tissue engineering.

Materials and methods

Ethics statement

The Ethics Committee of the First Affiliated Hospital of Chongqing Medical University approved all animal protocols. All surgeries were performed under appropriate anesthesia; each animal was housed in individual cage under standard conditions until they were confirmed to be recovering from anesthesia without pain. Mice were euthanized at the indicated time points by an intraperitoneal overdose of sodium pentobarbital (Sigma-Aldrich, USA). Every effort was made to minimize animal distress, after confirming that mice were not breathing, not beating heartbeat, and mydriasis, the ectopic masses were removed from the injection site of the nude mice.

Cell culture and chemicals

Human embryonic kidney (HEK) 293 and mouse MSC C3H10T1/2 cell lines were obtained from the American

Type Culture Collection (ATCC, Manassas, VA, USA). Human umbilical vein endothelial cells (HUVECs) were purchased from Procell Life Technology (Wuhan, China). All cell lines were housed in cell incubators and cultured in complete medium with 10% fetal bovine serum (FBS, Gibco, Australia), containing 100 U/mL penicillin and 100 mg/mL streptomycin. Unless indicated otherwise, all chemicals were purchased from Sigma-Aldrich.

Construction and generation of recombinant adenoviral vectors

Recombinant adenovirus vectors were generated using AdEasy technology as described in our previous studies.^{6,20,35–37} AdBMP9 was characterized previously,^{36,38} and AdGFP expressing green fluorescent protein (GFP) was used as empty control adenoviruses. For making silence H19 vectors, Gibson Assembly system was utilized to simultaneously assemble three small interfering RNAs (siRNAs) targeting mouse H19 and generation AdSimH19 expression red fluorescent protein (RFP).^{24,39} Recombinant adenovirus vectors were amplified in human embryonic kidney 293 (HEK-293) cells. Briefly, adenovirus stocks were obtained by harvesting cells when both cell density and fluorescence brightness were at appropriate levels, followed with high-speed centrifugation and repeated freeze–thaw cycles.

RNA isolation and quantitative PCR (qPCR)

Cell samples were washed with phosphate buffer saline (PBS) three times and the residual liquid was aspirated. Total RNA was extracted using an RNA extraction kit (AG21017, Accurate Biology, China) according to manufacturer's protocol. Then total RNA was subjected to reverse transcription using a reverse transcription kit (RT Master Mix for qPCR, HY-K0511, MCE, USA). CDNA was diluted with SYBR Green qPCR Master Mix (HY-K0523, MCE, USA) and subjected to following qPCR analysis with the using of CFX96 real-time PCR detection system (Bio-Rad, USA). The real-time qPCR program was as follows: 95 °C for 30 s, 95 °C for 5 s, and 60 °C for 30 s, repeating 40 cycles. *GAPDH* was used as a reference gene. All sample values were normalized to *GAPDH* expression using the $2^{-\Delta\Delta Ct}$ method. qPCR primer sequences are listed in Table S1.

Protein harvest and Western blot analysis

Protein extraction was performed using 2% sodium dodecyl sulfate (SDS) lysis buffer, which including 100 mM Tris–HCl, 100 mM β -mercaptoethanol, protease and phosphatase inhibitors (Roche, USA). Protein concentration was measured using BCA protein analysis kit (Beyotime, Beijing, China), then denatured by boiling for 10 min. Protein samples were separated by electrophoresis with Tris–glycine buffer and transferred carefully onto polyvinylidene difluoride (PVDF, Millipore, USA) membranes under dark conditions. Then PVDF membranes were blocked with 5% evaporated milk for 1 h and incubated overnight with primary antibodies against osteocalcin (OC, ab93876, Abcam, USA), Runx2 (#20700-1-AP, Proteintech, China), Collagen Type I (Col1a1, #14695-1-

AP, Proteintech, China), Notch1 (ab52627, Abcam, USA), p53 (ab1101, Abcam, USA), p-p53 (phospho S15) (ab223868, Abcam, USA) or *GAPDH* (#10494-1-AP, Proteintech, China). PVDF membranes were washed with Tris buffered saline Tween-20 (TBST) 3 times on a shaker for 10 min each time. Following this, membranes were incubated with corresponding horseradish peroxidase-conjugated (HRP) secondary antibody (goat anti-rabbit secondary antibody, 1:1000, Cell Signaling Technology, USA). Blotting is shown using Immobilon Western chemiluminescent HRP substrate (Millipore, USA). Relative protein expression was analyzed by Image Lab software using *GAPDH* protein as a control.

Alkaline phosphatase (ALP) analysis

MSCs were seeded in a 24-well plate with a density of 30%–40%, and stimulated with adenovirus respectively. For ALP staining, cells were fixed with 4% paraformaldehyde for 30 min, then, washed twice with PBS and stained with ALP Color Development Kit (Beyotime, China). Thirty minutes later, cells were observed under a bright field microscopy. As for quantitative analysis of ALP activity, cells in each treatment group were lysed by lysis buffer, then 5 μ L lysis buffer, 5 μ L substrate (BD Clontech), and 15 μ L Lupo Buffer were mixed and incubated in light-proof condition for 20 min followed with measuring chemiluminescence signals. ALP activity was normalized by total protein concentrations in each treatment group. Each assay condition was performed in triplicate, and the results were repeated in at least 3 independent experiments.

Alizarin red S staining

MSCs were seeded in 24-well cell culture plates and infected with indicated adenoviruses 24 h later. After confluence, cell medium was changed with osteogenic medium containing ascorbic acid (50 mg/mL) and β -glycerophosphate (10 mM) for 14 and 21 days. The mineralization nodules were assessed by Alizarin red S staining as previously described.^{5,6,10,20,38}

Flow cytometry analysis

The cell markers of C3H10T1/2 cells were detected using flow cytometry. C3H10T1/2 cells were seeded at a density of 2×10^6 /mL in a 6-well plate and stimulated with indicated adenovirus vectors. At indicated time points, cells were digested and collected in a 100- μ L cell suspension, followed with transferred to a flow cytometric tube. Then, cell suspensions were incubated with conjugated CD31 (BioLegend, USA) antibodies for 30 min at 4 °C in the dark condition. After being washed three times with PBS, the labeled cells were resuspended in 0.2 mL PBS and analyzed with the CytoFLEX system (Beckman Coulter, USA). The acquired data were analyzed by using CytExpert software (Beckman Coulter, USA).

Cell migration assays

MSCs were inoculated in the lower chamber of Transwell (24-well plate, 8.0 μ m, Jet Bio-Filtration) at a density of

30%–40%, and were transfected with different adenoviruses. The medium was changed on the second day of infection. When the MSC cell density reached 100%, the old medium was removed and washed 3 times with PBS, replace with fresh complete medium containing 5% FBS; replace the negative control group with serum-free complete medium, and replace the positive control group with complete medium containing 15% FBS. At the same time 2.5×10^4 HUVECs were seeded in the upper chamber of the Transwell. After culturing for 12 h, the upper chamber was taken out, the cells on the upper membrane were gently removed with a cotton swab, and then the upper chamber was fixed with 4% paraformaldehyde for 20 min. The cells on the bottom membrane were stained with 0.1% crystal violet staining solution (G1063, Solarbio, China) as previously reported.⁴⁰

Wound healing assays

Human umbilical vein endothelial cells (HUVEC) were seeded in the lower chamber of the Transwell (6-well plate, 0.4 μm , Jet Bio-Filtration, China) and cultured to a density of 100%. Meanwhile, MSCs infected with indicated adenovirus vectors were transferred into the upper chamber of the Transwell at a seeding density of 30%–40% individually, when the cell density reaches 100%, remove the old medium and wash three times with PBS, then replaced with fresh complete medium. HUVEC cells were drawn vertically along the diameter of the 6-well plate using a 200- μL pipette tip, and the MSCs prepared as described above were placed on the upper chamber of the Transwell co-culture. After 12 h, the scratch area of each group was recorded, and the change of the scratch area was calculated by Image J software.

Enzyme linked immunosorbent assay (ELISA)

The concentration of VEGFa in the supernatant of MSC cells transfected with adenovirus was detected using the ELISA kit (AF-02411M1, Ai Fang biological, China) following manufacturer's protocol. In brief, after confluence, supernatants in each treatment group were collected and subjected to optical density (OD) value determination at wavelength of 450 nm. All assays were performed in triplicate.

Magnetic beads sorting cells

The culture medium was changed 24 h after adenovirus infection. When close to confluence, cells were digested, resuspended and washed twice with PBS. Then, cells were resuspended in 100 μL PBS, mixed with 5 μL flow cytometry antibody (PE anti-mouse CD31 Antibody, BioLegend, USA) and incubated on ice for 30 min. After this, cells were washed twice with PBS and mixed with 100 μL of the prepared 1 \times buffer (MojoSort™ Buffer (5 \times), BioLegend, USA) and 10 μL magnetic beads (MojoSort™) Mouse anti-PE Nanobeads (BioLegend, USA), then incubated on ice for 30 min. After washing twice, cell suspension was subjected to the sorting magnetic column (MojoSort™ Magnet, BioLegend, USA) for 15 min. In order to obtain higher purity sorted cells, procedures were repeated twice. Use

complete medium to wash the wall of the flow cytometer to obtain the sorted positive cell suspension. Finally, positive and negative parts of the cell suspensions were identified by flow cytometric analysis.

Subcutaneous stem cell implantation

The use and care of animals in this study was approved by the Institutional Animal Care and Use Committee. All experimental procedures were performed in accordance with approved guidelines. The subcutaneous stem cell implantation procedure was performed as described previously. Briefly, C3H10T1/2 cells were infected with AdGFP, AdBMP9 and/or AdsimH19. When close to confluence, cells were resuspended with PBS at a density of 5×10^6 cells per 100 μL (100 μL per injection). Then cells were injected subcutaneously into both sides of nude mice flanks ($n = 3/\text{group}$, female, 5–6 weeks old). At the indicated time points, the animals were euthanized and the ectopic masses were removed from the injection site. After micro-CT scan, ectopic masses were fixed in 4% paraformaldehyde (Beyotime, China) at room temperature for 24 h, then immersed in ethylene diamine tetraacetic acid (EDTA) for decalcification. Replace the decalcification solution every 3 days until the tissue mass is completely softened, and then embedded in paraffin. Continuous 5 μm thick sections were obtained and subjected to histological staining.

Micro-CT analysis

Small animal Micro-CT (VivaCT80, CANCO Medical AG, Switzerland) was used to detect bone calcification inside the masses. Samples were fixedly placed in a custom-made foam holder. The scanning parameters were as follows: scanning time 30 min/sample, layer thickness spacing 10 μm , scanning working voltage 70 KV, current 114 μA . Scanco image analysis software was used to reconstruct and analyze the content of the masses.

Hematoxylin and eosin (H&E), Masson's trichrome staining and Safranin O-fast green staining

Paraffin-embedded sections were deparaffinized in xylene and then rehydrated in a graduated ethyl alcohol. Then, deparaffinized samples were subjected to hematoxylin and eosin (H&E), Masson's trichrome and Safranin O-fast green according to manufacturer's protocol as previously described.^{5,6,24,41} Histological evaluation was performed using a bright light microscope. Relative trabecular bone areas were analyzed by Image J software. Blood vessels were counted in high power (HP) field by three histologists following the double-blind principle.

Immunohistochemistry (IHC) assay

Cells were seeded on 24-well slides and processed according to the experimental protocol in cell immunohistochemistry experiments. At the indicated time points, cells were washed three times with PBS, then fixed with 4% paraformaldehyde. After blocking the cells with goat serum for 30 min, the cells were incubated with the corresponding

primary antibodies (VEGFA, #19003-1-AP and CD31, #28083-1-AP, Proteintech, China) at 4 °C overnight. Then, cells were incubated with secondary antibody for 1 h at room temperature and stained with 4',6-diamidino-2-phenylindole (DAPI).

For section immunohistochemistry experiments, sections were deparaffinized using xylene, rehydrated with graded ethanol, then treated with 3% hydrogen peroxide for 10 min, and boiled in antigen retrieval solution at 95–100 °C for 20 min, and blocked with normal goat serum for 30 min. Tissue sections were incubated with corresponding primary antibodies (VEGFR2, #26415-1-AP and CD31, #28083-1-AP, proteintech, China) overnight at 4 °C. After three washed with PBS, sections were incubated with biotin-labeled secondary antibody (SP0041, Solarbio, China) for 30 min, followed by streptavidin–horseradish peroxidase (HRP) conjugate for 20 min at room temperature. Staining without primary antibody was used as a negative control. Immunohistochemistry results were quantified using Image J software.

RNA immunoprecipitation (RIP) analysis

RIP analysis was done as previously characterized.^{24,42} In brief, C3H10T1/2 cells were lysed and subjected to RIP analysis with the use of Magna RIP™ RNA-Binding Protein Immunoprecipitation Kit (Millipore, Bedford, USA) following the manufacturer's protocols. Firstly, magnetic beads were pretreated with RIP wash buffer and incubated with p53 antibody (10442-1-AP, Proteintech, USA) for 30 min. Then, the magnetic bead p53 composites were incubated with cell lysis supernatant and RIP immunoprecipitation buffer overnight at 4 °C. Following this, RIP wash buffer was applied to wash sufficiently. Proteinase K buffer was utilized to detach RNA followed with RNA extraction. Finally, RNA fraction was isolated and subjected to perform qPCR analysis as described above.

Chromatin immunoprecipitation (ChIP) analysis

ChIP analysis was performed to determine the interacting of p-p53 and the Notch1 promoter and was carried out as previously described.^{43,44} Shortly, about 1×10^7 C3H10T1/2 cells were crosslinked with 1% formaldehyde for 10 min at room temperature and quenched with 0.125 M glycine (National Medicine Group, China) for 5 min. Then the cells were washed with PBS repeatedly. Immunoprecipitation cell pellets were lysed in lysis buffer containing 150 mM NaCl, 50 mM 2-hydroxyethyl (HEPES) (National Medicine Group, China), 1 mM EDTA, 0.1% SDS, 0.1% sodium deoxycholate, 1% Triton X-100, protease inhibitor cocktail (CWbiotech, China) for 10 min. Then, the pellet was subjected to sonication on the ice. After been confirmed the fragmentation in agarose gel, fragmented chromatin was incubated with primary p-p53 antibody (#9284, CST, USA) bound to the Pierce™ Protein A/G Agarose Beads (Thermo Fisher Scientific, Inc., USA) overnight at 4 °C. After immunoprecipitation, samples were eluted and reverse cross-linked overnight with DNA elution buffer containing TE buffer (10 mM Tris–HCl, 1 mM EDTA) at 65 °C, followed by RNase treatment (0.5 mg/mL) at 37 °C for 30 min and

proteinase K treatment (0.3 mg/mL) at 51 °C for 1 h. Finally, DNA was isolated and purified for qPCR analysis as described above.

Statistical analysis

All quantitative experiments were performed in triplicate and/or repeated three times. Data were expressed as mean \pm standard deviation ($m \pm SD$) and analyzed with GraphPad Prism (GraphPad Software, La Jolla, USA) version 8.0. Unpaired Student's *t* test (for two groups), one-way or two-way ANOVA (for multiple groups) were used followed by the Tukey–Kramer test. Values of $P < 0.05$ were considered statistically significant.

Results

H19 was highly expressed and essential in BMP9-induced MSCs differentiation

H19 was highly expressed in MSCs as we previously characterized.^{6,24} We firstly constructed silencing H19 adenovirus containing three different silence targets (Fig. S1A). Adenovirus mediated transduction of BMP9 and/or silencing H19 could efficiently infect MSCs (Fig. S1B). With the stimulation of BMP9, the expression levels of H19 were close to the expression levels of housekeeping gene β -Actin, which indicated the high expression level of H19 in MSCs (Fig. S1C). Subsequently, we confirmed the silencing efficiency of AdsimH19; the results showed that AdSimH19 could efficiently decrease the expression level of H19 (Fig. S1D) and not influence the expression of BMP9 in protein level (Fig. S1Ea,b).

Then, we characterized the effects of down-regulation of H19 on BMP9-induced osteogenic differentiation of MSCs. ALP staining (Fig. S2Aa) and ALP reading (Fig. S2Ab) showed that down-regulation of H19 inhibited BMP9-induced early-stage osteogenic differentiation of MSCs. As for late-stage osteogenic differentiation of MSCs, Alizarin staining (Fig. S2B) showed that down-regulation of H19 inhibited BMP9-induced matrix mineralization both in 2 weeks and 3 weeks. Meanwhile, Western blot analysis found that down-regulation of H19 dramatically reduced BMP9-induced key osteogenic differentiation transcription factor Runx2 expression at protein level (Fig. 2Ca), and quantitative analysis showed the same trend. As for osteogenic differentiation marker, Western blot (Fig. S2Da) and quantitative analysis (Fig. S2Db) results found that down-regulation of H19 dramatically inhibited BMP9-induced OC and Col1a1 expressions. These results indicated the essential role of H19 in BMP9-induced osteogenic differentiation of MSCs.

Down-regulation of H19 attenuated BMP9-induced angiogenesis of MSCs

We firstly determined the effects of down-regulation H19 on BMP9-induced angiogenesis of MSCs. To address the effect of BMP9-induced MSCs angiogenesis on HUVECs migration, Transwells with 8- μ m diameter mesh membranes were used for co-culture. The simulated diagram was shown in

Figure 1Aa, and the results showed that with the stimulation of BMP9, MSCs secreted growth factors induced HUVECs migration, and down-regulation of H19 attenuated these effects (Fig. 1Ab), quantitative analysis showed the same trend (Fig. 1Ac). Wound healing assay was also carried out (Fig. 1B). As shown in Figure 1Ba, MSCs stimulated with BMP9 and/or simH19 were cultured in the upper chamber with 3- μ m diameter mesh membrane, and HUVECs were cultured in the lower chamber, where wound healing assay was taken out. The results showed that, with the stimulation of BMP9, HUVECs would close the wound more quickly

compared with the control group. However, down-regulation of H19 could inhibit this effect at both 12 and 24 h. Quantitative analysis showed the same trend (Fig. 1Bc). Furthermore, we determined VEGFa concentration in supernatant in each group, and found that BMP9-induced VEGFa secretion could be inhibited by down-regulation of H19 (Fig. 1Ca). IHC staining showed that BMP9-induced expression of VEGFa and CD31 positive cells could be inhibited by down-regulation of H19 (Fig. 1Cb). These results suggested that down-regulation of H19 could attenuate BMP9-induced angiogenesis of MSCs.

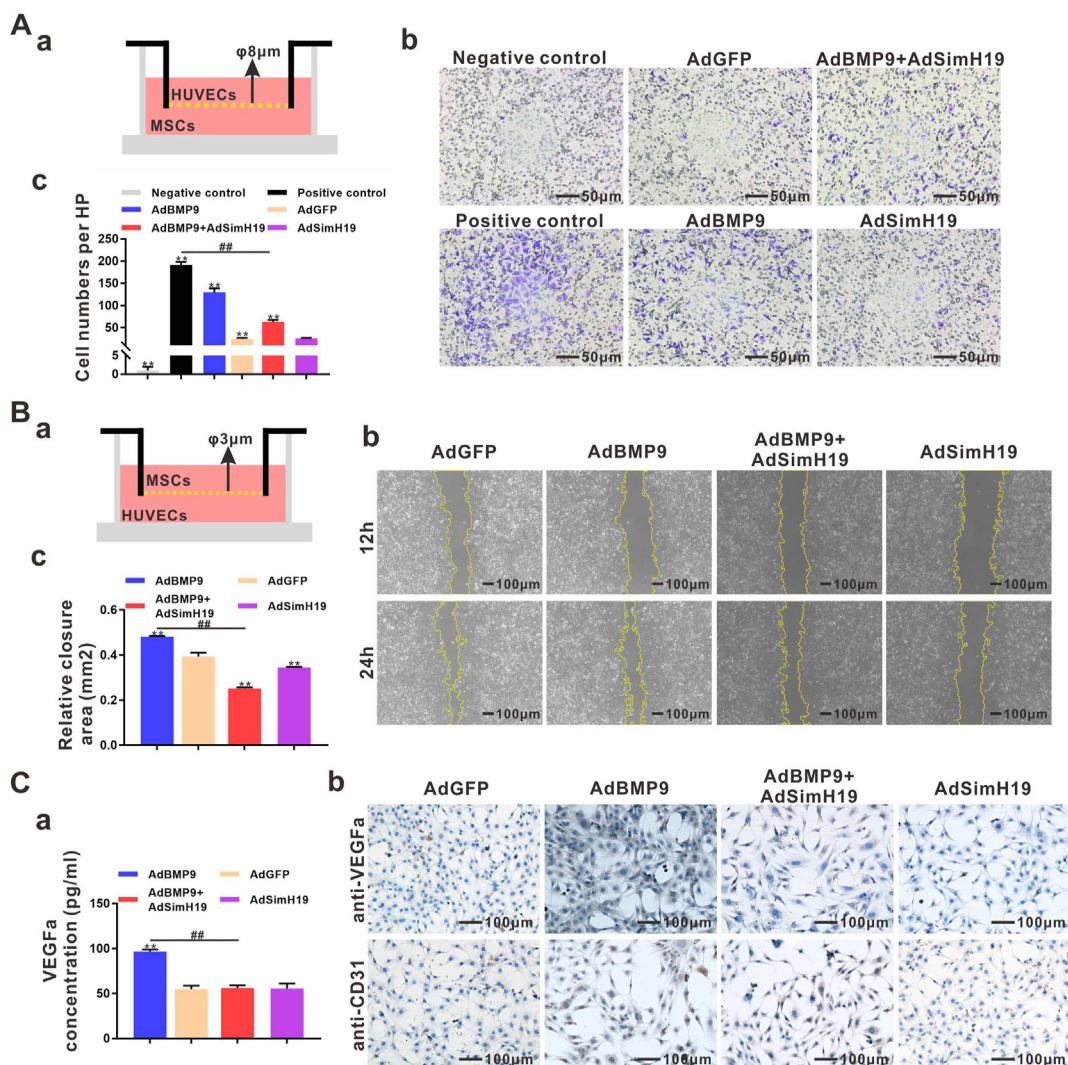


Figure 1 Silencing H19 attenuated BMP9-induced osteogenic differentiation of MSCs. (A) Silencing H19 inhibited BMP9-induced HUVECs migration. A diagram summarized co-culture system of MSCs and HUVECs (a). Viable cells were detected by crystal violet staining (b), MSCs in the upper chamber were used as negative control and HUVECs in the lower chamber were used as positive control, scale bar, 50 μm . Quantitative analysis of viable cells (c) showed that BMP9-induced HUVECs migration was inhibited by silencing H19. (B) Silencing H19 inhibited BMP9-induced HUVECs migration by wound closure. A diagram summarized co-culture system of MSCs and HUVECs (a). Cell closure at 12 and 24 h were presented (b) and quantitative analysis of closure areas showed that BMP9-induced HUVECs migration to close the wound was inhibited by silencing H19 (c). Scale bar, 100 μm . (C) Silencing H19 inhibited BMP9-induced VEGFa and the production of CD31⁺ cells. BMP9-induced secretion of VEGFa was determined by ELISA on day 5 after adenovirus infection (a), BMP9-induced VEGFa secretion was inhibited by silencing H19. The cytoplasmic VEGFa and CD31 expressions were identified by IHC (b) on day 5 after BMP9 stimulation and the results showed that BMP9 mediated VEGFa and CD31 expressions were inhibited by AdSimH19 mediated down-regulation of H19, scale bar, 100 μm . The one-way ANOVA, ** $P < 0.01$, compared with control (AdGFP) group, ## $P < 0.01$, compared with indicated group.

BMP9-induced production of CD31⁺ cells was indispensable for BMP9-induced bone formation

As an endothelial cell marker, CD31 is specific for endothelial differentiation. To confirm the angiogenesis potential of BMP9, flow cytometry was utilized to identify CD31⁺ cells on day 0, 1, 3, 5, and 7, respectively. We found that, with the stimulation of BMP9, CD31⁺ cells proportion increased gradually from day 0 to day 5, and decreased slightly on day 7 (Fig. 2Aa,b). To further identify the function of CD31⁺ cells in BMP9-induced bone formation, we screened CD31⁺ cells with flow cytometry. The morphologies of CD31⁺ cells and CD31⁻ cells were exhibited in Figure 2Ba, and flow cytometry identifying the efficiency of screening was shown in Figure 2Bb. CD31⁻ MSCs stimulated with BMP9 were subcutaneously implanted and the ectopic masses were obtained 4 weeks after implantation. Micro-CT reconstruction morphologies were shown in Figure 2Ca. Volume analysis found that compared with the normal group, CD31⁻ cells formed smaller ectopic bone masses (Fig. 2Cb) with lower BV/TV ration (Fig. 2Cc). Histologically, less trabecular bone, blood vessels and more undifferentiated cells were found in CD31⁻ cells group compared with normal group. These results indicated that BMP9-induced CD31⁺ cells are indispensable for BMP9-induced bone formation.

Down-regulation of H19 attenuates BMP9-induced angiogenesis and followed ectopic bone formation

To further clarify the influence of down-regulation of H19 on BMP9-induced angiogenesis of MSCs, CD31⁺ cells were identified by flow cytometry with the stimulation of BMP9 with or without AdSimH19. We found that down-regulation of H19 dramatically attenuated BMP9-induced production of CD31⁺ cells (Fig. 3Aa). The quantitative analysis found that BMP9-induced up-regulation of CD31⁺ cells production could be down-regulated by silencing H19 (Fig. 3Ab). These results indicated that H19 regulated BMP9-induced angiogenesis by decreasing the production of CD31⁺ cells. Then, subcutaneously implantation of MSCs was carried out *in vivo*. Three dimensional (3D) reconstruction images of different time points' ectopic masses were presented in Figure 3Ba. Bone volumes analysis showed that BMP9-induced bone volume increasing started in two weeks and reached a peak in 4 weeks, however, down-regulation of H19 delayed this phenomenon significantly (Fig. 3Bb). As for bone mineral density (BMD) analysis, we found that down-regulation of H19 decreased BMP9-induced BMD significantly in 2, 4 and 6 weeks respectively (Fig. 3Bc). Histologically (Fig. 3C), we found that both AdBMP9 group and AdBMP9 + AdsimH19 group had trabecular bone formation and undifferentiated MSCs, however, AdBMP9 + AdsimH19 group almost had no blood vessels formation compared with AdBMP9 group. When it moved to 4 weeks, trabecular bone increased in both groups and AdBMP9 group with higher proportion compared with AdBMP9 + AdsimH19 group. Meanwhile, more blood vessels formation in both trabecular bone and undifferentiated area in AdBMP9 group compared with AdBMP9 + AdsimH19 group. In 6 weeks, abundant vascularized bone formation in AdBMP9 group, however, fewer vascularized trabecular bone mixed

with a mass of undifferentiated MSCs were found in AdBMP9 + AdsimH19 group. Trichrome and Safranin O-fast green staining in 4 weeks and 6 weeks confirmed the phenomenon (Fig. 4A). What was more, IHC staining confirmed blood vessels formation with staining with VEGFR2⁺ cells in both groups. As shown in Figure 4B, compared with AdBMP9 groups, angiogenesis potential of MSCs decreased dramatically in AdBMP9 + AdsimH19 groups in 2, 4 and 6 weeks, respectively. Quantitative analysis of proportion of trabecular bone proportions and numbers of blood vessels were significantly higher in AdBMP9 groups when compared with AdBMP9 + AdsimH19 groups in 2, 4 and 6 weeks, respectively (Fig. 4C). These results implied that down-regulation of H19 inhibited BMP9-induced osteogenesis–angiogenesis coupling.

H19 regulates BMP9-induced angiogenesis by potentiating p53 mediated Notch1 activation

As p53 is one of the key downstream targets of H19, we firstly detected the expressions of p53 when down-regulation H19 in BMP9-induced MSCs differentiation. We found that down-regulation of H19 did not influence total p53 expression, however, p-p53 expression was dramatically down-regulated by AdSimH19 in BMP9-induced MSCs differentiation (Fig. 5Aa–c). Then RIP analysis was carried out to confirm the interaction of H19 and p53, the confirmation of p53 and GAPDH was confirmed by protein precipitation (Fig. 5Ba), input and post-precipitation of H19 and p53 protein were pull-down by p53 antibody, IgG was used as control (Fig. 5Bb). Immunoprecipitation products were subjected to RNA extraction and purification, and the expressions of H19 were detected by RT-qPCR. We found that the expression of H19 in IP group was dramatically higher than IgG group (Fig. 5Bc), which indicated the binding interaction of H19 and p53 protein.

As we previously characterized that Notch1 mediated BMP9-induced angiogenesis,⁵ we detected Notch1 activation when down-regulation of H19 in BMP9-induced MSCs differentiation. We found that downregulation of H19 inhibited BMP9-induced *Notch1* mRNA expression (Fig. 6Aa) and dramatically inhibited NICD1 expression at protein level (Fig. 6Ab,c). Then, we confirmed down-regulation of Notch1 signaling with DAPT dramatically decreased BMP9-induced production of CD31⁺ cells (Fig. 6Ba,b). Therefore, we speculated that p-p53 may regulate Notch1 signaling activation and ChIP analysis was carried out. Genomic DNA was extracted and confirmed on gel (Fig. 6Ca). The expression of p-p53 after precipitation was confirmed by Western blot analysis, GAPDH was used as control. Three pairs of primers were designed according to the promoter area sequence and distributed at the top, middle and lower area, respectively (Fig. 6Bc). After the precipitation, DNA was extracted and subjected to PCR analysis. We found that compared with IgG group, all three fragments DNA sequences were upregulated dramatically and the top fragment with the highest level (Fig. 6Bd). These results indicated the combination interaction of p-p53 and *Notch1* promoter.

Taken together, our results suggested that H19 regulates BMP9-induced angiogenesis of MSCs by regulating the phosphorylation of p53 and p-p53 binds on the Notch1

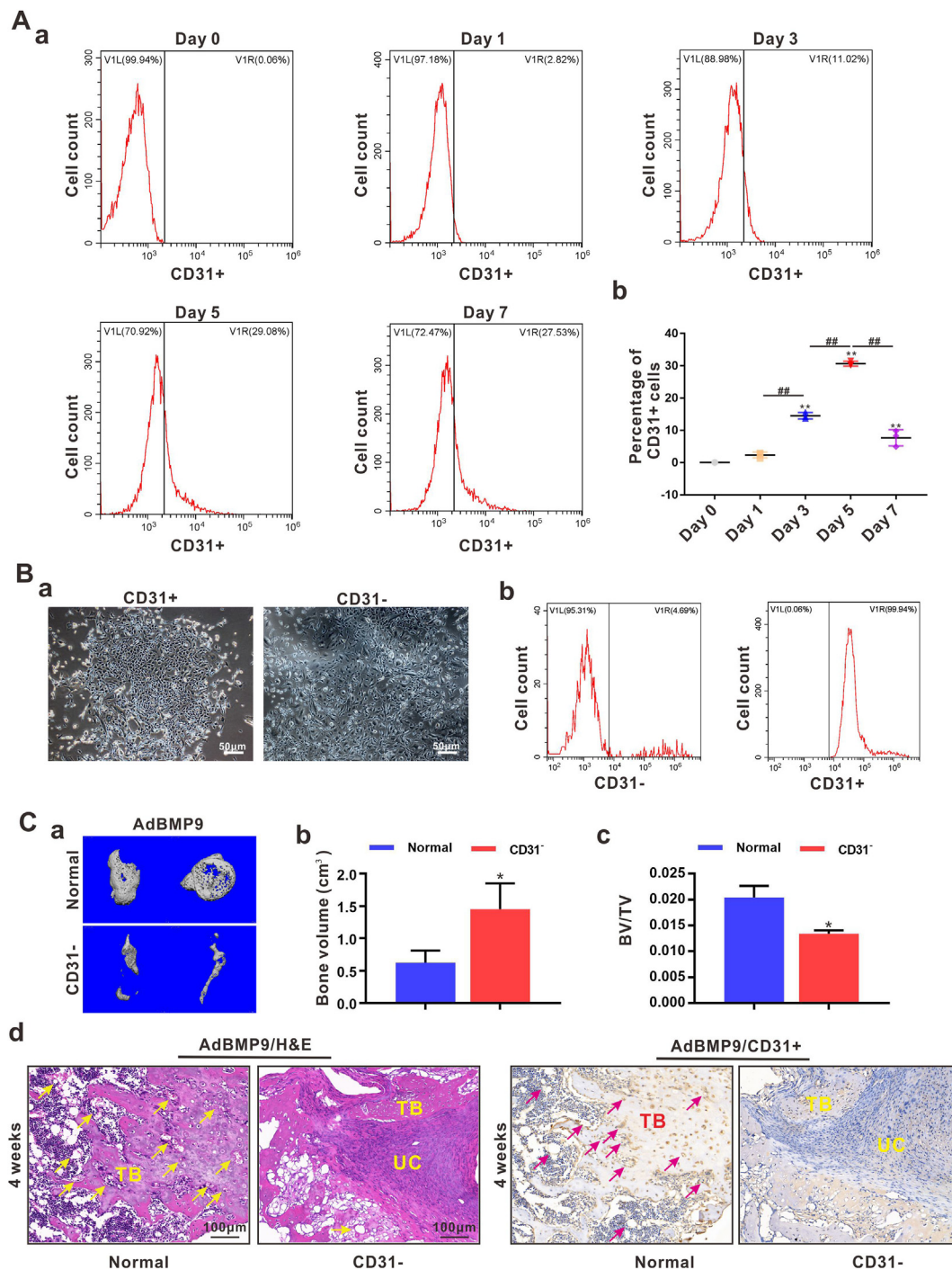


Figure 2 BMP9-induced production of CD31⁺ cells was indispensable for BMP9-induced bone formation. **(A)** Proportions of CD31⁺ cells increased gradually with the stimulation of BMP9. MSCs were infected with AdBMP9 and subjected to flow cytometry screening for CD31⁺ cells, proportions of CD31⁺ cells were recorded at day 0, 1, 3, 5, and 7, respectively (a), day 0 means without BMP9 treatment. Quantitative analysis (b) of three independent tests showed that with the stimulation of BMP9, CD31⁺ cells proportions increased from day 3 to day 7, and reach the peak on day 5. The one-way ANOVA, ** $P < 0.01$, * $P < 0.05$, compared with control (AdGFP) group, ## $P < 0.01$, compared with indicated group. **(B)** Morphologies (a) and identification of CD31⁺ and CD31⁻ cells (b). CD31⁺ cells were cells identified as positive with flow cytometry, and CD31⁻ cells were all other types of cells except CD31⁺ cells, scale bar 50 µm. **(C)** Decreased osteogenic differentiation potential of MSCs lack of CD31⁺ cells. MSCs lack of CD31⁺ cells and normal MSCs were infected with AdBMP9, 48 h later, cells were re-suspended and subcutaneously injected in the nude mice, 4 weeks later, ectopic masses were harvested and subjected to following analysis. Micro-CT reconstructed ectopic masses (a), bone volume (b) and BV/TV (c) analysis showed that, although MSCs lack of CD31⁺ cells obtained larger volume with the stimulation of BMP9, trabecular bone volume was statically less than normal MSCs. Histologically (d), H&E staining showed that normal MSCs formed trabecular bone with abundant blood vessels with the treatment of

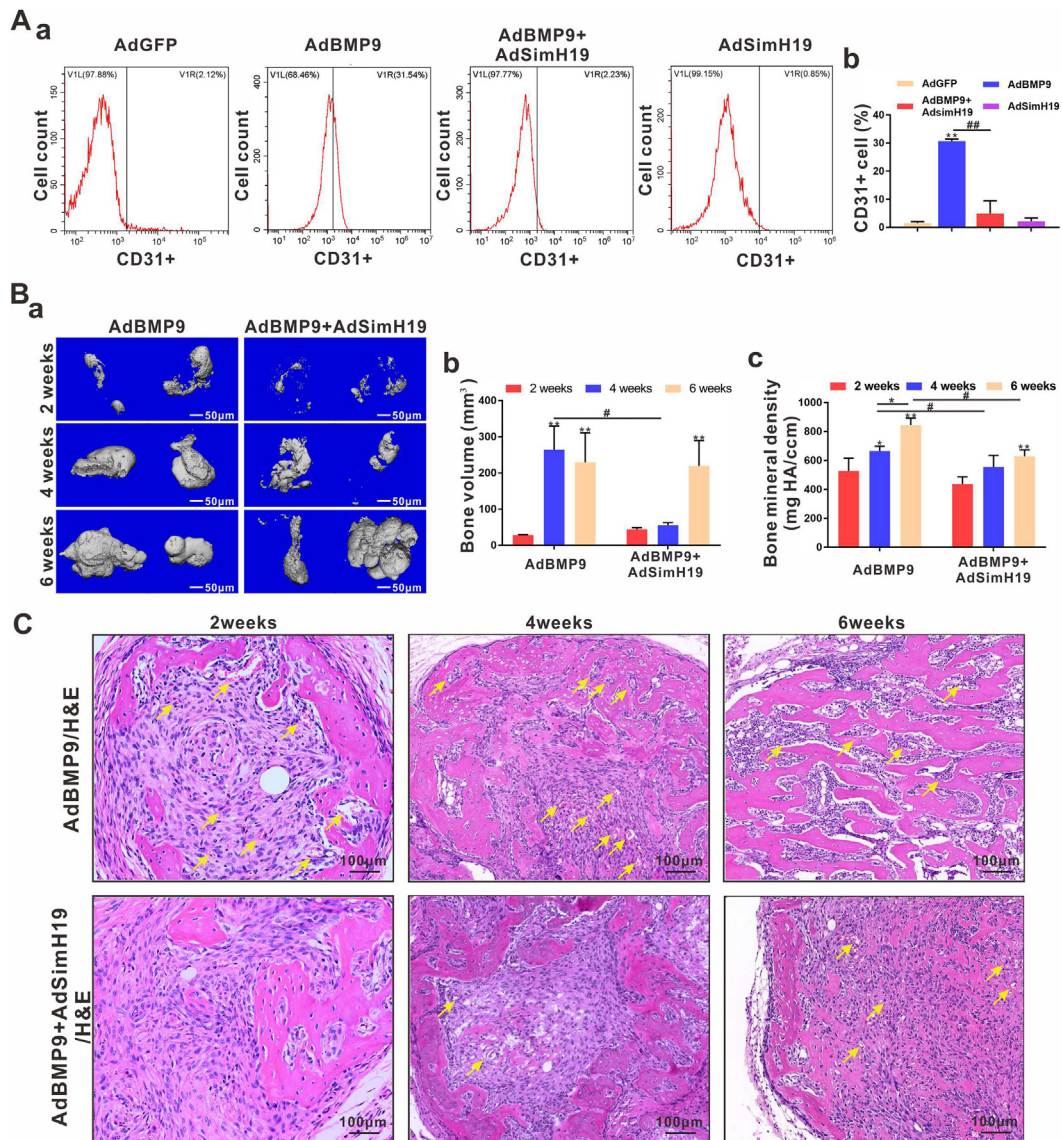


Figure 3 Down-regulation of H19 attenuated BMP9-induced angiogenesis and followed ectopic bone formation. **(A)** Silencing H19 attenuated BMP9-induced production of CD31⁺ cells. MSCs were treated with AdBMP9 and/or AdSimH19; AdGFP was used as control. Five days after infections, each treatment group was subjected to flow cytometry for screening CD31⁺ cells (a), quantitative analysis (b) showed that BMP9 up-regulated CD31⁺ cells proportion significantly compared with control group, and silencing H19 blocked CD31⁺ cells generation significantly compared with AdBMP9 group. The one-way ANOVA, ** $P < 0.01$, compared with control (AdGFP) group, ^{###} $P < 0.01$, compared with indicated group. **(B, C)** Silencing H19 attenuated BMP9-induced bone and blood vessels formation *in vivo*. MSCs were treated with AdBMP9 and/or AdSimH19; AdGFP was used as control. At indicated time points, ectopic masses (no obvious mass formation in AdGFP and AdSimH19 groups) were subjected to micro-CT and histological analysis. Reconstructed ectopic masses at 2, 4 and 6 weeks were shown (a). Bone volume analysis (b) showed that silencing H19 delayed BMP9-induced bone volume increasing, and bone mineral density analysis (c) showed that silencing H19 statistically decreased BMP9-induced bone mature in 4 and 6 weeks. The one-way ANOVA, ** $P < 0.01$, * $P < 0.05$, compared with 2 weeks, ^{###} $P < 0.05$, compared with indicated group. Histologically, in AdBMP9 group, obvious blood vessels were found in 2 weeks, and vascularized trabecular bone formation gradually from 4 to 6 weeks. When silencing H19, no obvious blood vessels formation in 2 weeks, and less trabecular bone and more undifferentiated cells were found in both 4 weeks and 6 weeks compared with AdBMP9 group. Scale bar 100 µm.

BMP9 for 4 weeks, MSCs lack of CD31⁺ cells formed less trabecular bone with a mass of undifferentiated cells without obvious blood vessels formation. IHC staining showed the undifferentiated cells were CD31⁻ cells. TB, trabecular bone, UC, undifferentiated cells, arrows indicated blood vessels. Unpaired Student's *t* test, * $P < 0.05$, compared with normal group.

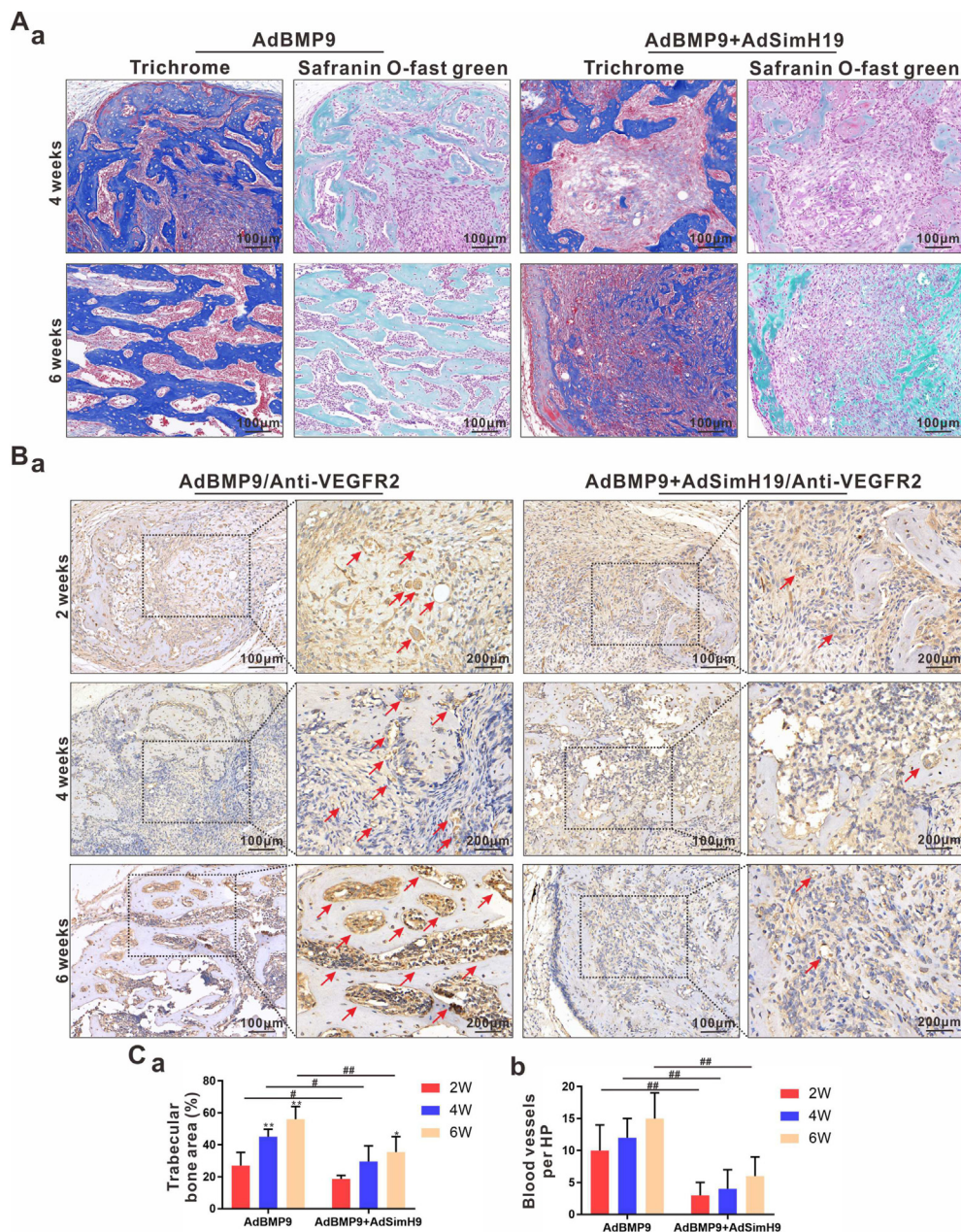


Figure 4 Trichrome, Safranin O-fast green staining and IHC assay for detecting trabecular bone and angiogenic activities. **(A)** Trichrome and Safranin O-fast green staining were used to identify the collagen formation, when down-regulation H19, less and more immature trabecular bone were found compared with AdBMP9 group. **(B)** IHC assay for detecting blood vessels. VEGFR2 were used for detecting angiogenic activities in 2, 4 and 6 weeks. VEGFR2⁺ cells mainly expressed around blood vessels, and more blood vessels were identified in AdBMP9 group compared with AdBMP9 + AdSimH19 group. Dotted box indicated the area in high power field. **(C)** Quantitative analysis of trabecular bone area (a) and number of blood vessels per high power field (HP) (b) showed decreased angiogenic activities and vascularized bone formation abilities when silencing H19. The two-way ANOVA, ** $P < 0.01$, * $P < 0.05$, compared with 2 weeks, ### $P < 0.05$, compared with indicated group.

promoter area then promoting the activation of Notch1 (Fig. 6D).

Discussion

Bone tissue engineering is potential for the treatment of clinical critical-size bone defects or nonunion of fractures,

however, it is still a challenge to obtain vascularized tissue-engineered bone.^{45,46} As one of the most osteogenic BMPs, BMP9 hold the potential to induce MSCs both osteogenesis and angiogenesis, but the mechanisms in detail are not clarified.^{4,35} In the present study, we clarified that H19 regulated BMP9-induced angiogenesis by promoting phosphorylation of p53, and phosphorylated p53 interacted with

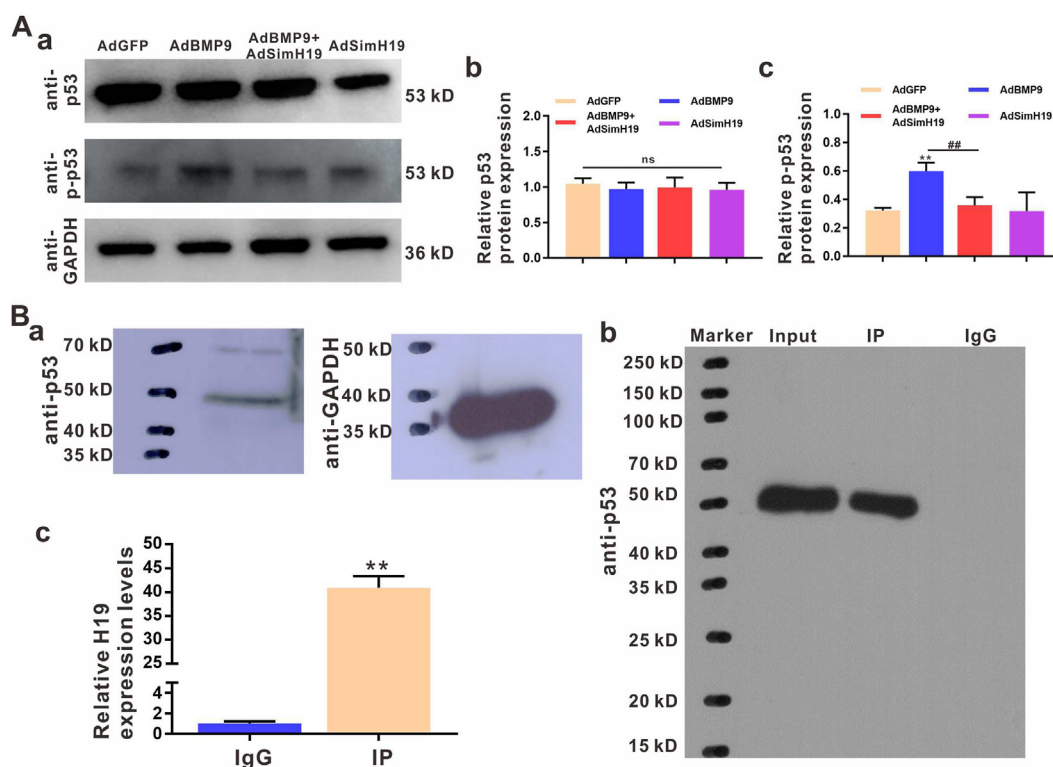


Figure 5 H19 promoted BMP9-induced phosphorylation of p53 by directly interaction. **(A)** Down-regulation of H19 attenuated BMP9-induced phosphorylation of p53. Total p53 and p-p53 were detected by Western blot (a), no statistical difference was found among each treatment group for the expressions of total p53 (b). As for p-p53, BMP9-induced up-regulation of p-p53 was dramatically inhibited by silencing H19. The one-way ANOVA, $**P < 0.01$, compared with control (AdGFP) group, $^{##}P < 0.01$, compared with indicated group. **(B)** Interaction of p53 and H19 by RIP analysis. The expression of p53 was confirmed before immunoprecipitation, and GAPDH was used as reference protein (a). Post immunoprecipitation (IP), Western blot analysis with p53 antibody was used to detecting p53, 10% input, and IgG group were used as controls (c). H19 expression levels in IP and IgG groups were determined by RT-qPCR(c), the levels of H19 were presented as fold enrichment in anti-RUNX2 relative to IgG immunoprecipitations. Unpaired Student's *t* test, $**P < 0.01$, compared with normal group.

the promoter area of *Notch1* to regulate the activation of *Notch1*. These results applied new evidence for clarifying the mechanisms of BMP9 mediated angiogenesis and osteogenesis coupling, which could promote the construction of BMP9-induced vascularized tissue-engineered bone.

MSCs can be isolated from many tissues and undergo self-renew, which hold the potential to differentiate into multiple lineages, including osteogenic, chondrogenic, angiogenic and adipogenic lineages, etc.^{3,47} Recently, the heterogeneity of stem cells has aroused scientists' attention and such heterogeneity decreases the reproducibility of research or treatment.⁴⁸ Therefore, the updating and characterization of unambiguous molecular markers for specific situation were identified as an effective way to promote the efficiency of stem cell based therapy.^{48–50} CD31 is one of the cell surface markers, which is negative in MSCs and positive in endothelial cells.^{49,51} In the present study, we found that the production of CD31⁺ cells increased with the stimulation of BMP9 and insufficient CD31⁺ cells dramatically decreased BMP9-induced osteogenesis and angiogenesis. What was more, we characterized that CD31⁺ cells mainly gathered around the blood vessels in BMP9-induced bone formation. These results

indicated the essential role of CD31⁺ cells during MSCs based vascularized bone formation.

The *H19* gene encodes a 2.3-kb non-coding mRNA which is strongly expressed during embryogenesis. As an imprinted cluster, H19 conserved on mouse chromosome 7 and human chromosome 11p15 and belongs to an imprinted cluster.^{52,53} Although the H19-IGF2 imprinting mechanisms have been clarified, recent studies indicated new regulatory functions of H19 in both physiology and pathology processes.^{14,15,30,54–56} Specifically, except competing endogenous RNA (ceRNA) mechanism, H19 mediated epigenetic mechanisms, including DNA methylation, histone modification and chromatin remodeling were reported more recently.^{21,57–59} Our previous studies clarified the regulatory function of H19 in BMP2 induced phosphorylation of Runx2 and inhibited hypertrophic differentiation.²⁴ Here we identified that H19 could interact with p53 and promote p53 phosphorylation, which further regulated BMP9 mediated angiogenesis of MSCs. To the best of our knowledge, this is the first time to report the regulation function of H19 in angiogenesis of MSCs. Taken previously identified regulatory function of H19 in osteogenic differentiation of MSCs and this study together,^{6,20,22,23,60} we have reason to

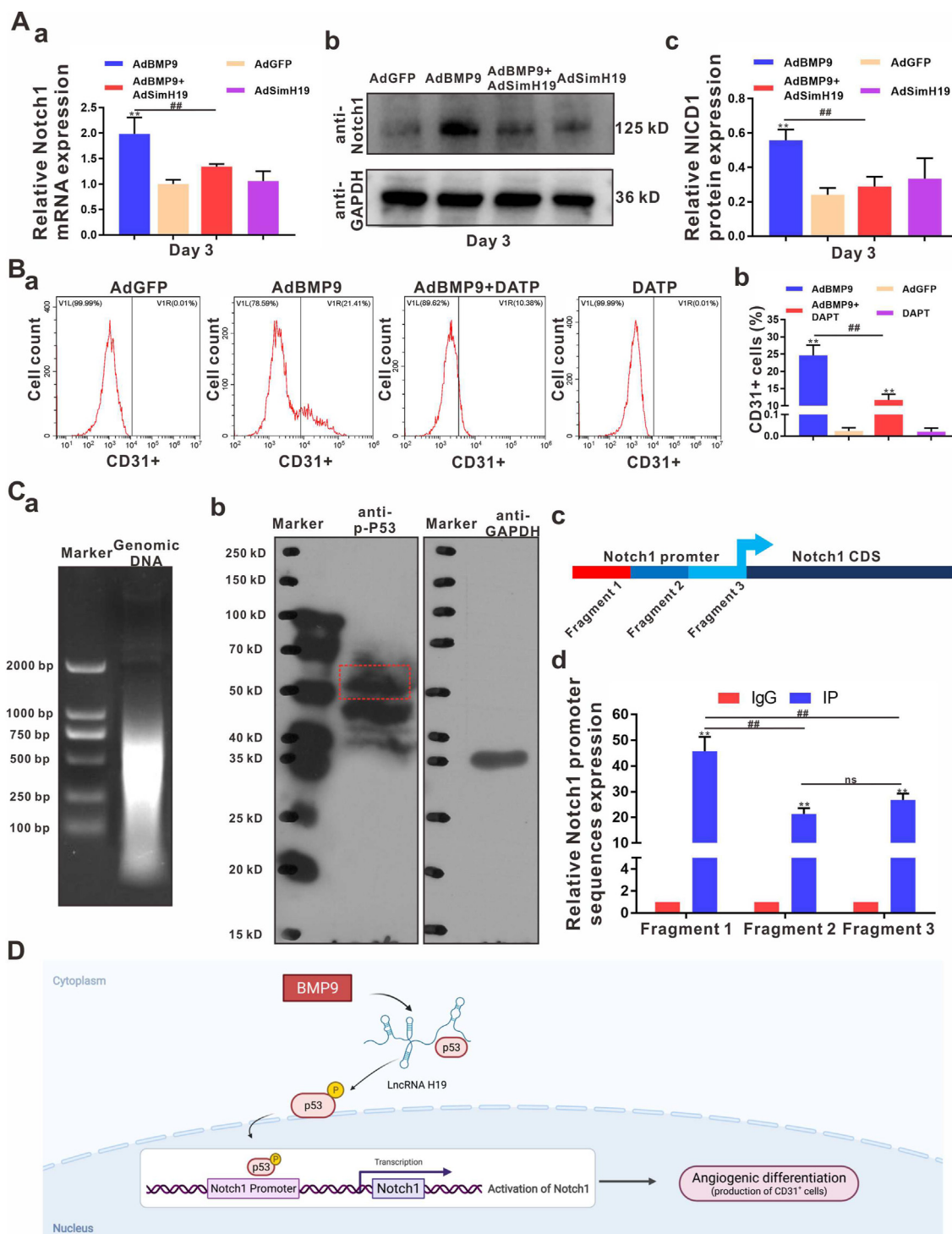


Figure 6 Phosphorylated p53 promoted Notch1 expression by interacting with Notch1 promoter. **(A)** Down-regulation of H19 attenuated *Notch1* expressions at both mRNA and protein level. MSCs in each treatment group were subjected to RT-qPCR on day 3, BMP9 dramatically up-regulated *Notch1* mRNA expression compared with control group, and silencing H19 statistically inhibited the up-regulation of *Notch1* (b). Western blot analysis (b) was carried out three days after adenovirus infection, quantitative analysis showed that BMP9-induced up-regulation of Notch1 was inhibited by silencing H19 (c). The one-way ANOVA, $**P < 0.01$, compared with control (AdGFP) group, $^{###}P < 0.01$, compared with indicated group. **(B)** γ -secretase inhibitor DAPT attenuated BMP9-induced production of CD31⁺ cells. MSCs were induced with AdBMP9; AdGFP was used as control. 24 h after infection, γ -secretase inhibitor DAPT or DMSO was added into the medium and flow cytometry was carried out on day 5 (a), quantitative analysis (b) showed that DAPT significantly inhibited BMP9-induced production of CD31⁺ cells. The one-way ANOVA, $**P < 0.01$, compared with control (AdGFP) group, $^{###}P < 0.01$, compared with indicated group. **(C)** Phosphorylated p53 promote Notch1 expression by interacting with Notch1 promoter. About 1×10^7 C3H10T1/2 cells were lysed and subjected to sonication, fragmented DNA was detected on 1%

believe the important role of H19 in osteogenesis and angiogenesis coupling process, which could be an essential target for promoting BMP9 mediated tissue engineering bone.

The tumor suppressor p53 is induced in cells in response to genotoxic and oncogenic stress and functions as a guardian of the genome by repairing damaged DNA or promoting pro-apoptotic process. Germline mutations in the *TP53* gene encoding p53 are responsible for Li-Fraumeni syndrome (LFS), which was characterized as a variety of tumor types, including osteosarcoma (OS), soft tissue sarcoma, breast cancer, brain tumor, leukemia, and adrenocortical carcinoma.⁶¹ Lee et al³⁰ identified that p53 mutant impairs osteoblast differentiation by down-regulation of H19, which resulted in osteosarcoma. However, the function of p53 in MSCs and osteogenic differentiation process are rarely reported. Recently, the essential roles of basal p53 expression in MSCs integrity, osteogenic differentiation fate, etc., were clarified, which indicated the regulatory function of p53 in MSCs differentiation.^{26,27,62,63} Velletri et al²⁶ reported that p53 status negatively regulated osteoprotegerin (OPG) amount and further regulate bone remodeling. Meanwhile, Boregowda et al²⁷ reported that p53 regulated MSCs cell fate and survival decisions under physiologic oxygen levels, which indicated the physiological function of p53 in MSCs. In addition, Lengner et al²⁵ found that Mdm2-p53 axis regulated osteoblast osteogenic differentiation and skeletal development by regulating Runx2 activation. In our study, we found total p53 was highly expressed in MSCs, and phosphorylation activation of p53 was identified with the stimulation of BMP9. In addition, we clarified that the phosphorylation activation of p53 was mediated by H19, which applied new evidence for the regulatory function of H19-p53 axis.^{34,63}

Osteogenesis and angiogenesis are highly coupled during the process of bone formation. We previously characterized that insufficient angiogenic signal would inhibit trabecular bone formation and promote adipogenesis in BMP9-induced bone formation.⁶⁴ Next, we found that Notch1 signaling activation mediated BMP9-induced angiogenesis and confirmed the essential role of Notch1 in BMP9-induced vascularization.⁵ Here, we firstly identified Notch1 signaling inhibition could attenuate BMP9-induced production of CD31⁺ cells. Then, we further clarified the upstream signaling of Notch1 and found that phosphorylated p53 could be translocated to the nuclear and interacting with the promoter of *Notch1* then promoting *Notch1* expression. Be similar with our results, Lefort et al⁶⁵ also reported that *Notch1* was one of the p53 target genes. In addition, the crosstalk between Notch signaling and p53

could inhibit tumor angiogenesis,⁶⁶ however, our results indicated that p53-Notch1 axis could promote angiogenesis of MSCs. This difference may suggest the function of p53 is different between tumorigenesis and MSCs osteogenic differentiation.

As an effective regulator, H19 was reported to regulate Notch1 signaling activation in various ways. We previously characterized that H19 acted as ceRNA to sponge microRNAs (miRs) which targeted *Notch1*, however, it is difficult to confirm a certain functional miR. Hadji et al⁶⁷ reported that H19 regulated Notch1 activation by regulating p53 expression in calcific aortic valve mineralization, and confirmed the interaction of p53 and Notch1 promoter by ChIP assay. Be similar with Hadji's findings, we found that H19 promoted the phosphorylation of p53 and phosphorylated p53 upregulated *Notch1* expression. Though we identified that phosphorylated p53 could bind on the promoter area of Notch1, we did not find the interaction site of phosphorylated p53 and Notch1 promoter, we speculate that other transcription factors may participate in this process.^{68,69} Taken these researches together, H19 may regulate the activation of Notch1 signaling through multiple mechanisms, and the predominant mechanism differs in different physiology and/or pathological process.

In summary, clarifying the mechanism of BMP9-induced angiogenesis of MSCs is essential for the construction of BMP9 based vascularized tissue engineering bone. As a functional lncRNA, the regulatory mechanisms of H19 in BMP9-induced angiogenesis are far from clarified. Here, we characterized the regulatory axis of H19-p-p53-Notch1 in BMP9-induced angiogenesis of MSCs, which offer an alternative role of p53 mediated Notch1 activation in BMP9 mediated tissue engineering bone.

Conflict of interests

The authors declare no conflict of interests.

Funding

The reported work was supported by the National Natural Science Foundation of China, PRC (No. #82002312 and #81972069). This project was also supported by Science and Technology Research Program of Chongqing Education Commission, PRC (No. #KJQN202100431 and #KJZD-M202100401), Candidate of Tip-Top Talent of the First Affiliated Hospital of Chongqing Medical University, PRC (No. BJRC2021-04) and Natural Science Foundation of Chongqing Science and Technology Commission, PRC (No. #cstc2018jcyjAX0088). Dr Liao is a postdoctoral fellow of

agarose gel (a). After immunoprecipitation, p-p53 was detected by Western blot assay and GAPDH was used as control (b). A diagram indicated the distribution of three pairs of primers for detection about 2000 bp prior to the coding sequence (CDS) of *Notch1* (c). RT-qPCR for detecting the enrichment of *Notch1* promoter area respectively, IgG was used as control. The two-way ANOVA, ** $P < 0.01$, compared with control (IgG) group, ### $P < 0.01$, compared with indicated group, ns, not significant. (D) A diagram summarizing the main findings of the research. H19 regulates BMP9-induced angiogenesis of MSCs by regulating the phosphorylation of p53, p-p53 interacts with *Notch1* promoter and promotes the activation of Notch1.

Chongqing Medical University. Funding sources were not involved in the study design, in the collection, analysis and interpretation of data; in writing of the report; and in the decision to submit the paper for publication.

Data availability statement

All datasets generated for this study are included in the article and [Supplementary materials](#).

Acknowledgements

We are grateful for the support of Life Science Institute of Chongqing Medical University.

Appendix A. Supplementary data

Supplementary data to this article can be found online at <https://doi.org/10.1016/j.gendis.2022.04.013>.

References

- Collon K, Gallo MC, Lieberman JR. Musculoskeletal tissue engineering: regional gene therapy for bone repair. *Biomaterials*. 2021;275:120901.
- Ho-Shui-Ling A, Bolander J, Rustom LE, et al. Bone regeneration strategies: engineered scaffolds, bioactive molecules and stem cells current stage and future perspectives. *Biomaterials*. 2018;180:143–162.
- Soldner F, Jaenisch R. Stem cells, genome editing, and the path to translational medicine. *Cell*. 2018;175(3):615–632.
- Mostafa S, Pakvasa M, Coalson E, et al. The wonders of BMP9: from mesenchymal stem cell differentiation, angiogenesis, neurogenesis, tumorigenesis, and metabolism to regenerative medicine. *Genes Dis*. 2019;6(3):201–223.
- Liao J, Wei Q, Zou Y, et al. Notch signaling augments BMP9-induced bone formation by promoting the osteogenesis-angiogenesis coupling process in mesenchymal stem cells (MSCs). *Cell Physiol Biochem*. 2017;41(5):1905–1923.
- Liao J, Yu X, Hu X, et al. LncRNA H19 mediates BMP9-induced osteogenic differentiation of mesenchymal stem cells (MSCs) through Notch signaling. *Oncotarget*. 2017;8(32):53581–53601.
- Luther G, Wagner ER, Zhu G, et al. BMP-9 induced osteogenic differentiation of mesenchymal stem cells: molecular mechanism and therapeutic potential. *Curr Gene Ther*. 2011;11(3):229–240.
- Tang N, Song WX, Luo J, et al. BMP-9-induced osteogenic differentiation of mesenchymal progenitors requires functional canonical Wnt/beta-catenin signalling. *J Cell Mol Med*. 2009;13(8B):2448–2464.
- Kang Q, Sun MH, Cheng H, et al. Characterization of the distinct orthotopic bone-forming activity of 14 BMPs using recombinant adenovirus-mediated gene delivery. *Gene Ther*. 2004;11(17):1312–1320.
- Hu N, Jiang D, Huang E, et al. BMP9-regulated angiogenic signaling plays an important role in the osteogenic differentiation of mesenchymal progenitor cells. *J Cell Sci*. 2013;126(Pt 2):532–541.
- Huang H, Weng H, Chen J. m⁶A modification in coding and non-coding RNAs: roles and therapeutic implications in cancer. *Cancer Cell*. 2020;37(3):270–288.
- Goodall GJ, Wickramasinghe VO. RNA in cancer. *Nat Rev Cancer*. 2021;21(1):22–36.
- Jain AK. Emerging roles of long non-coding RNAs in the p53 network. *RNA Biol*. 2020;17(11):1648–1656.
- Moulton T, Crenshaw T, Hao Y, et al. Epigenetic lesions at the H19 locus in Wilms' tumour patients. *Nat Genet*. 1994;7(3):440–447.
- Taniguchi T, Sullivan MJ, Ogawa O, et al. Epigenetic changes encompassing the IGF2/H19 locus associated with relaxation of IGF2 imprinting and silencing of H19 in Wilms tumor. *Proc Natl Acad Sci U S A*. 1995;92(6):2159–2163.
- Ripoche MA, Kress C, Poirier F, et al. Deletion of the H19 transcription unit reveals the existence of a putative imprinting control element. *Genes Dev*. 1997;11(12):1596–1604.
- Zhou Z, Hossain MS, Liu D. Involvement of the long noncoding RNA H19 in osteogenic differentiation and bone regeneration. *Stem Cell Res Ther*. 2021;12(1):74.
- Ghafouri-Fard S, Esmaeili M, Taheri M. H19 lncRNA: roles in tumorigenesis. *Biomed Pharmacother*. 2020;123:109774.
- Raveh E, Matouk IJ, Gilon M, et al. The H19 long non-coding RNA in cancer initiation, progression and metastasis - a proposed unifying theory. *Mol Cancer*. 2015;14:184.
- Liao J, Xiao H, Dai G, et al. Recombinant adenovirus (AdEasy system) mediated exogenous expression of long non-coding RNA H19 (lncRNA H19) biphasic regulating osteogenic differentiation of mesenchymal stem cells (MSCs). *Am J Transl Res*. 2020;12(5):1700–1713.
- Liu Y, Li G, Zhang JF. The role of long non-coding RNA H19 in musculoskeletal system: a new player in an old game. *Exp Cell Res*. 2017;360(2):61–65.
- Huang Y, Zheng Y, Jin C, et al. Long non-coding RNA H19 inhibits adipocyte differentiation of bone marrow mesenchymal stem cells through epigenetic modulation of histone deacetylases. *Sci Rep*. 2016;6:28897.
- Liang WC, Fu WM, Wang YB, et al. H19 activates Wnt signaling and promotes osteoblast differentiation by functioning as a competing endogenous RNA. *Sci Rep*. 2016;6:20121.
- Dai G, Xiao H, Zhao C, et al. LncRNA H19 regulates BMP2-induced hypertrophic differentiation of mesenchymal stem cells by promoting Runx2 phosphorylation. *Front Cell Dev Biol*. 2020;8:580.
- Lengner CJ, Steinman HA, Gagnon J, et al. Osteoblast differentiation and skeletal development are regulated by Mdm2-p53 signaling. *J Cell Biol*. 2006;172(6):909–921.
- Velletri T, Huang Y, Wang Y, et al. Loss of p53 in mesenchymal stem cells promotes alteration of bone remodeling through negative regulation of osteoprotegerin. *Cell Death Differ*. 2021;28(1):156–169.
- Boregowda SV, Krishnappa V, Strivelli J, et al. Basal p53 expression is indispensable for mesenchymal stem cell integrity. *Cell Death Differ*. 2018;25(4):679–692.
- Levine AJ. p53: 800 million years of evolution and 40 years of discovery. *Nat Rev Cancer*. 2020;20(8):471–480.
- Shermane Lim YW, Xiang X, Garg M, et al. The double-edged sword of H19 lncRNA: insights into cancer therapy. *Cancer Lett*. 2021;500:253–262.
- Lee DF, Su J, Kim HS, et al. Modeling familial cancer with induced pluripotent stem cells. *Cell*. 2015;161(2):240–254.
- Li DY, Busch A, Jin H, et al. H19 induces abdominal aortic aneurysm development and progression. *Circulation*. 2018;138(15):1551–1568.
- Geng H, Bu HF, Liu F, et al. In inflamed intestinal tissues and epithelial cells, interleukin 22 signaling increases expression of H19 long noncoding RNA, which promotes mucosal regeneration. *Gastroenterology*. 2018;155(1):144–155.
- Li Y, Ma HY, Hu XW, et al. LncRNA H19 promotes triple-negative breast cancer cells invasion and metastasis through the p53/TNFAIP8 pathway. *Cancer Cell Int*. 2020;20:200.

34. Phermthai T, Pokathikorn P, Wichitwiengrat S, et al. P53 mutation and epigenetic imprinted *IGF2/H19* gene analysis in mesenchymal stem cells derived from amniotic fluid, amnion, endometrium, and Wharton's jelly. *Stem Cells Dev.* 2017; 26(18):1344–1354.
35. Zhang L, Luo Q, Shu Y, et al. Transcriptomic landscape regulated by the 14 types of bone morphogenetic proteins (BMPs) in lineage commitment and differentiation of mesenchymal stem cells (MSCs). *Genes Dis.* 2019;6(3):258–275.
36. Lee CS, Bishop ES, Zhang R, et al. Adenovirus-mediated gene delivery: potential applications for gene and cell-based therapies in the new era of personalized medicine. *Genes Dis.* 2017;4(2):43–63.
37. Luo J, Deng ZL, Luo X, et al. A protocol for rapid generation of recombinant adenoviruses using the AdEasy system. *Nat Protoc.* 2007;2(5):1236–1247.
38. Xiao H, Wang X, Wang C, et al. BMP9 exhibits dual and coupled roles in inducing osteogenic and angiogenic differentiation of mesenchymal stem cells. *Biosci Rep.* 2020;40(6):BSR20201262.
39. Deng F, Chen X, Liao Z, et al. A simplified and versatile system for the simultaneous expression of multiple siRNAs in mammalian cells using Gibson DNA Assembly. *PLoS One.* 2014; 9(11):e113064.
40. Liao J, Wei Q, Fan J, et al. Characterization of retroviral infectivity and superinfection resistance during retrovirus-mediated transduction of mammalian cells. *Gene Ther.* 2017; 24(6):333–341.
41. Xiao P, Zhu Z, Du C, et al. Silencing Smad7 potentiates BMP2-induced chondrogenic differentiation and inhibits endochondral ossification in human synovial-derived mesenchymal stromal cells. *Stem Cell Res Ther.* 2021;12(1):132.
42. Yuan JH, Yang F, Wang F, et al. A long noncoding RNA activated by TGF- β promotes the invasion-metastasis cascade in hepatocellular carcinoma. *Cancer Cell.* 2014;25(5):666–681.
43. Li X, Wei Z, Yu H, et al. Secretory autophagy-induced bladder tumour-derived extracellular vesicle secretion promotes angiogenesis by activating the TPX2-mediated phosphorylation of the AURKA-PI3K-AKT axis. *Cancer Lett.* 2021;523:10–28.
44. Jiang HT, Deng R, Deng Y, et al. The role of Serpina3n in the reversal effect of ATRA on dexamethasone-inhibited osteogenic differentiation in mesenchymal stem cells. *Stem Cell Res Ther.* 2021;12(1):291.
45. Yin S, Zhang W, Zhang Z, et al. Recent advances in scaffold design and material for vascularized tissue-engineered bone regeneration. *Adv Healthc Mater.* 2019;8(10):e1801433.
46. Johnson EO, Troupis T, Soucacos PN. Tissue-engineered vascularized bone grafts: basic science and clinical relevance to trauma and reconstructive microsurgery. *Microsurgery.* 2011; 31(3):176–182.
47. Li JJ, Hosseini-Beheshti E, Grau GE, et al. Stem cell-derived extracellular vesicles for treating joint injury and osteoarthritis. *Nanomaterials.* 2019;9(2):E261.
48. Hayashi Y, Ohnuma K, Furue MK. Pluripotent stem cell heterogeneity. *Stem Cells Heterog Nov Concepts.* 2019;1123:71–94.
49. Calloni R, Cordero EA, Henriques JA, et al. Reviewing and updating the major molecular markers for stem cells. *Stem Cells Dev.* 2013;22(9):1455–1476.
50. Yamanaka S. Pluripotent stem cell-based cell therapy-promise and challenges. *Cell Stem Cell.* 2020;27(4):523–531.
51. Chambers SEJ, Pathak V, Pedrini E, et al. Current concepts on endothelial stem cells definition, location, and markers. *Stem Cells Transl Med.* 2021;10(suppl 2):S54–S61.
52. Gabory A, Ripoche MA, Yoshimizu T, et al. The H19 gene: regulation and function of a non-coding RNA. *Cytogenet Genome Res.* 2006;113(1–4):188–193.
53. Gabory A, Jammes H, Dandolo L. The H19 locus: role of an imprinted non-coding RNA in growth and development. *Bioessays.* 2010;32(6):473–480.
54. Tran VG, Court F, Duputié A, et al. H19 antisense RNA can up-regulate Igf2 transcription by activation of a novel promoter in mouse myoblasts. *PLoS One.* 2012;7(5):e37923.
55. Keniry A, Oxley D, Monnier P, et al. The H19 lincRNA is a developmental reservoir of miR-675 that suppresses growth and Igf1r. *Nat Cell Biol.* 2012;14(7):659–665.
56. De Martino M, Forzati F, Marfella M, et al. HMGA1P7-pseudogene regulates H19 and Igf2 expression by a competitive endogenous RNA mechanism. *Sci Rep.* 2016;6:37622.
57. Tsai MC, Manor O, Wan Y, et al. Long noncoding RNA as modular scaffold of histone modification complexes. *Science.* 2010; 329(5992):689–693.
58. Gao LM, Xu SF, Zheng Y, et al. Long non-coding RNA H19 is responsible for the progression of lung adenocarcinoma by mediating methylation-dependent repression of CDH1 promoter. *J Cell Mol Med.* 2019;23(9):6411–6428.
59. Sasaki H, Ishihara K, Kato R. Mechanisms of Igf2/H19 imprinting: DNA methylation, chromatin and long-distance gene regulation. *J Biochem.* 2000;127(5):711–715.
60. Huang Y, Zheng Y, Jia L, et al. Long noncoding RNA H19 promotes osteoblast differentiation via TGF- β 1/Smad3/HDAC signaling pathway by deriving miR-675. *Stem Cells.* 2015; 33(12):3481–3492.
61. Malkin D, Li FP, Strong LC, et al. Germ line p53 mutations in a familial syndrome of breast cancer, sarcomas, and other neoplasms. *Science.* 1990;250(4985):1233–1238.
62. Yi L, Lu C, Hu W, et al. Multiple roles of p53-related pathways in somatic cell reprogramming and stem cell differentiation. *Cancer Res.* 2012;72(21):5635–5645.
63. Velletri T, Xie N, Wang Y, et al. P53 functional abnormality in mesenchymal stem cells promotes osteosarcoma development. *Cell Death Dis.* 2016;7:e2015.
64. Wang J, Liao J, Zhang F, et al. NEL-like molecule-1 (Nell1) is regulated by bone morphogenetic protein 9 (BMP9) and potentiates BMP9-induced osteogenic differentiation at the expense of adipogenesis in mesenchymal stem cells. *Cell Physiol Biochem.* 2017;41(2):484–500.
65. Lefort K, Mandinova A, Ostano P, et al. Notch1 is a p53 target gene involved in human keratinocyte tumor suppression through negative regulation of ROCK1/2 and MRCKalpha kinases. *Genes Dev.* 2007;21(5):562–577.
66. Kim SB, Chae GW, Lee J, et al. Activated Notch1 interacts with p53 to inhibit its phosphorylation and transactivation. *Cell Death Differ.* 2007;14(5):982–991.
67. Hadji F, Boulanger MC, Guay SP, et al. Altered DNA methylation of long noncoding RNA H19 in calcific aortic valve disease promotes mineralization by silencing NOTCH1. *Circulation.* 2016;134(23):1848–1862.
68. Pellatt LJ, Rice S, Mason HD. Phosphorylation and activation of AMP-activated protein kinase (AMPK) by metformin in the human ovary requires insulin. *Endocrinology.* 2011;152(3): 1112–1118.
69. Ardito F, Giuliani M, Perrone D, et al. The crucial role of protein phosphorylation in cell signaling and its use as targeted therapy (review). *Int J Mol Med.* 2017;40(2):271–280.